

Communication

Role of Longitudinal Temperature Gradients in Eliminating Interleaving Inclusions in Casting of Monocrystalline Silicon Ingots

Lindong Li and Changbo Fu * 

Key Laboratory of Nuclear Physics and Ion–Beam Application (MOE), Institute of Modern Physics, Fudan University, Shanghai 200433, China

* Correspondence: cbfu@fudan.edu.cn

Abstract: Infrared analysis reveals the presence of interwoven inclusions, primarily comprised of silicon nitride and silicon carbide, in the casting process of monocrystalline silicon ingots. This study investigates how the longitudinal temperature gradient affects the removal of inclusions during the casting of monocrystalline silicon ingots through simulations and comparative experiments. Two monocrystalline silicon ingots were cast, each using different longitudinal temperature gradients: one employing smaller gradients and the other conventional gradients. CGSim (Version Basic CGSim 23.1) simulation software was utilized to analyze the melt flow and temperature distribution during the growth process of quasi–monocrystalline silicon ingots. The findings indicate that smaller longitudinal temperature gradients lead to a more robust upward flow of molten silicon at the solid–liquid interface, effectively carrying impurities away from this interface and preventing their inclusion formation. Analysis of experimental photoluminescence and IR results reveals that although inclusions may not be observed, impurities persist but are gradually displaced to the top of the silicon melt through a stable growth process.

Keywords: infrared; inclusions; CGSim; quasi–monocrystalline



Citation: Li, L.; Fu, C. Role of

Longitudinal Temperature Gradients in Eliminating Interleaving Inclusions in Casting of Monocrystalline Silicon Ingots. *Crystals* **2024**, *14*, 471. <https://doi.org/10.3390/cryst14050471>

Academic Editor: Shouxun Ji

Received: 19 April 2024

Revised: 10 May 2024

Accepted: 14 May 2024

Published: 17 May 2024



Copyright: © 2024 by the authors. Licensee MDPI, Basel, Switzerland. This article is an open access article distributed under the terms and conditions of the Creative Commons Attribution (CC BY) license (<https://creativecommons.org/licenses/by/4.0/>).

1. Introduction

Methods for growing quasi–monocrystalline silicon ingots have rapidly expanded in recent years, mainly achieving improvements in the understanding of the behavior of defects and the proportions of single crystals. Yield is the main indicator in achieving mass production. The main factors affecting the yield include the proportion of single crystals, the defect density, and the elimination of inclusions. Inclusions have a negative impact on the slicing yield and efficiency of solar cells. Cutting silicon bricks that contain impurities can easily cause wire breakage [1,2]. Inclusions often appear in infrared flaw–detection maps, caused by the accumulation of impurity particles during the growth of the monocrystalline silicon cast. There have been many studies conducted on inclusions, including their elemental analysis and their impact on dislocations. Zhou et al. [3] discovered that shadows are formed by small, dispersed impurity particles capable of inducing dislocations, sub–grain boundaries, and strip–shaped grains along the (110) direction. The authors of [4] suggest that inter–woven shadows primarily comprise silicon carbide and silicon nitride. Tsoutsouva et al. [5] reported that impurities such as carbon, oxygen, and nitrogen tend to precipitate within and near sub–boundaries, often leading to dislocation defects. Liu et al. [6] analyzed the distributions of carbon, oxygen, and iron impurities in quasi–single–crystal silicon wafers containing shadows.

Shadows adversely affect the cutting efficiency and yield of solar cells. The process of slicing silicon bricks containing impurities can easily result in wire breakage [1,2]. Moreover, impurity–induced reductions in the base diffusion length can lead to performance

degradation in solar cells [7]. The elimination of inclusion is therefore a necessary condition for the industrialization of quasi-monocrystalline silicon. In the early stages of the development of polycrystalline silicon technology, inclusions were also found in silicon ingots. For example, Zhang et al. [8] eliminated inclusions in cast polycrystalline silicon by increasing the G/V value (G is the near-interface temperature gradient, V is the growth rate), strengthening the melt convection front at the solidification interface, and maintaining a relatively flat solid–melt interface. However, these researchers believe that the inclusions were microcrystalline and not attributed to any impurity. Previous studies reported that carbon content can be reduced by optimizing airflow [9–14], but did not provide guidance on eliminating inclusions.

In the present study, the impact of the longitudinal temperature gradient on the growth process of quasi-monocrystalline silicon was studied through transient global simulation. The photoluminescence (PL) and infrared (IR) detection results of the monocrystalline silicon bricks show the influence of the two different longitudinal temperature gradients. It is evident that a reduced longitudinal temperature gradient is advantageous in reducing the inclusion of quasi-monocrystalline silicon bricks. A lower longitudinal temperature gradient offers a method to decrease inclusions in 1300 kg (G8-sized) monocrystalline silicon ingots.

2. Materials and Methods

Boron-doped monocrystalline silicon ingots weighing 1300 kg (G8-sized) were grown in a directional-solidification ingot furnace. The schematic diagram of the used experimental casting furnace is shown in Figure 1. The top and bottom heaters were separately controlled. Thermocouples TC1 and TC2 were respectively installed on the top and bottom of the furnace hot zone. The temperature settings of the thermocouples served to adjust the power of the corresponding heaters. Retention of seeds at the melting end was achieved using a low bottom temperature, which was controlled by bottom heat dissipation and bottom heater power. Seeds used for comparative experiments were cut from (100) Czochralski (Cz) silicon cylindrical rods and prepared as described by Tang [15,16]. A single-crystal round silicon rod was rotated by 15° before square rod preparation. Square rod cutting was carried out at 25 mm intervals, resulting in a seed thickness of 25 mm. Adjacent seeds were flipped 180° and then placed flat at the bottom of a crucible of size 1370 mm \times 1370 mm \times 420 mm. The damaged surface layer of the seed crystals was removed using HF and HNO₃. A 1300 kg (G8-sized) silicon ingot requires 64 seeds with a size of 166 mm \times 166 mm \times 25 mm. Control of the final melting stage by both the bottom temperature and melting speed ensured that the retention thickness of the seeds was close to 15 mm. Different growth process profiles, obtained from the temperature settings of the bottom thermocouples, were used to cast two monocrystalline silicon ingots with a weight of 1300 kg. Glass rods were used to measure the growth rate. The resulting ingots were cut into 64 bricks, as shown in Figure 2. Samples taken from the bricks in the middle of each ingot were evaluated for inclusion detection using a PL imaging system (BT Imaging, Redfern, Australia) and IR measurements. PL imaging, a non-intrusive technique, was employed to inspect silicon brick samples. This method involves illuminating the entire surface of the sample with an external light source, inducing luminescence emission within the sample. An infrared (IR) camera was utilized to detect and record this emission, analogous to capturing a picture of the luminescing sample. The utilization of optical signals for both excitation and detection renders PL imaging a non-contact technique suitable for evaluating various silicon brick sample arrays.

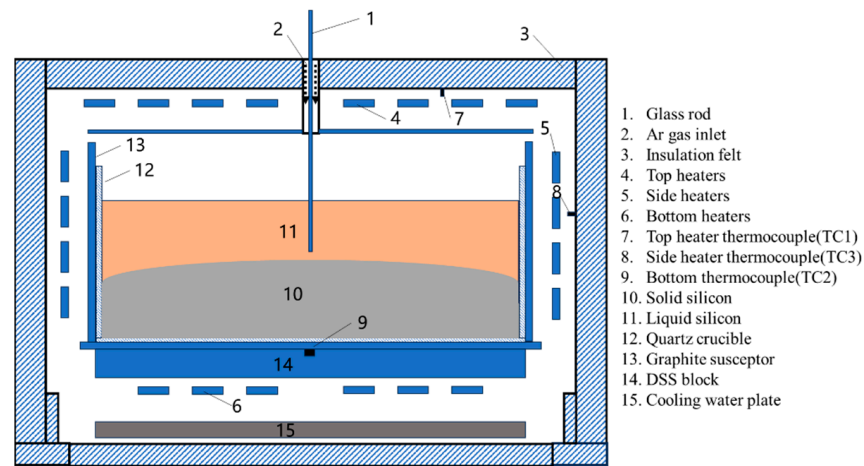


Figure 1. Schematic diagram of 1300 kg (G8-size) thermal zone.

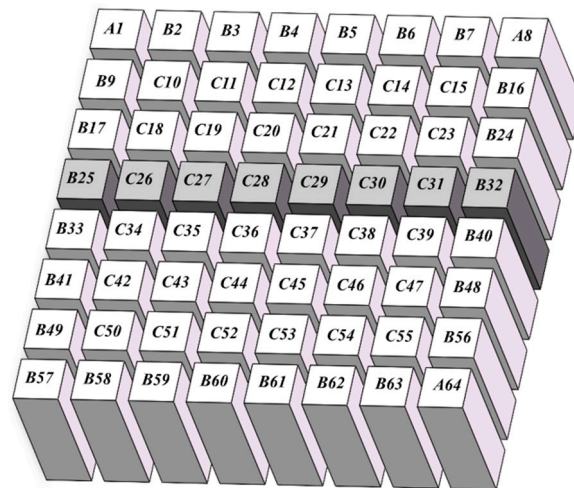


Figure 2. Schematic diagram of locations of bricks No. 25–32 within an ingot.

Similarly, IR detection is a non-contact evaluation technique employed for identifying regions with high-recombination centers within silicon blocks. Impurity distribution patterns within the blocks can be observed through the transmission of infrared light. IR testing is commonly employed as a standard procedure for analyzing impurity concentrations within silicon, following the guidelines outlined in the GB/T 13584–2011 standard [17].

CGSim simulated the flow of molten silicon near the solid-melt interface during the growth process. Figure 3 depicts a furnace model drawn based on the actual structure of the experimental casting furnace used for simulation. A two-dimensional model was constructed to replicate the real furnace's configuration. The simulation employed a numerical method that combined finite-element and finite-volume approaches. Key parameters utilized in simulating the growth of monocrystalline silicon ingots included crucible dimensions of 1370 mm × 1370 mm × 420 mm, an ingot mass of 1300 kg, and a furnace pressure of 0.06 MPa. Various simulations were carried out with different bottom temperatures. The simulation results of the growth process for the two monocrystalline silicon ingots align with the actual temperature parameters observed during casting tests.

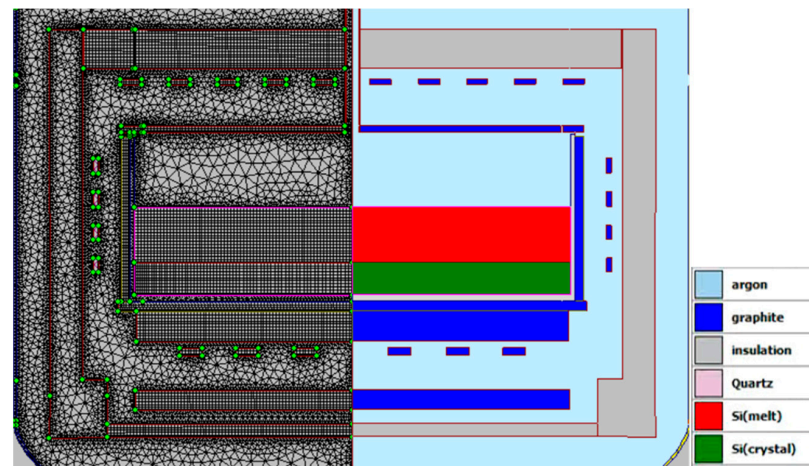


Figure 3. Schematic of furnace (right) and calculation grid (left).

The growth recipes for the two ingots used for simulation and experimentation are shown in Figure 4. It can be seen that due to the same top temperature and higher bottom temperature, the growth of the bottom temperature of ingot 2 is higher than that of ingot 1. Additionally, the longitudinal temperature gradient throughout the growth process of silicon ingot 2 appears to be less pronounced than that observed in silicon ingot 1.

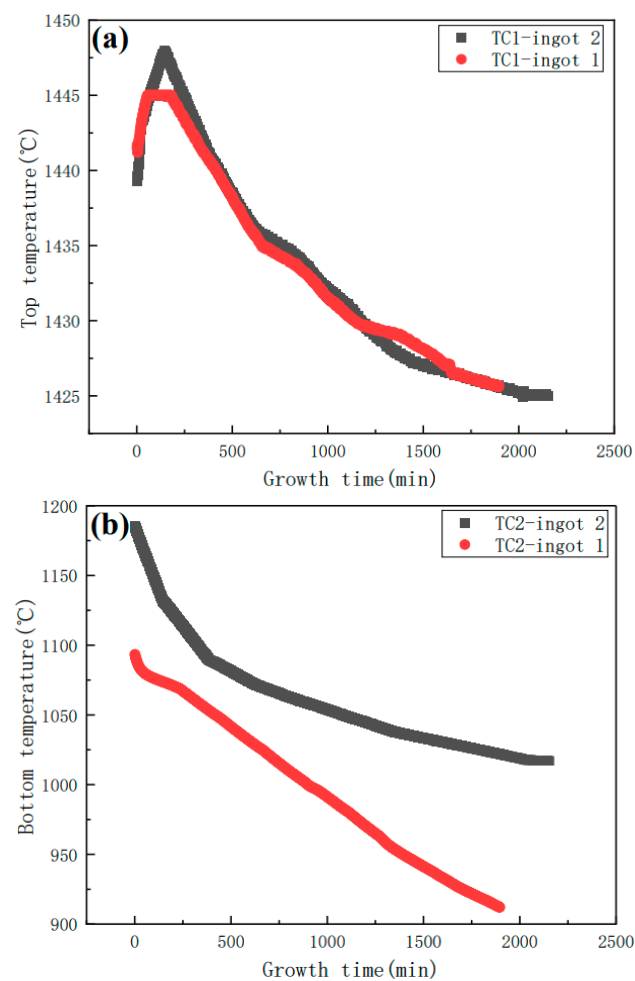


Figure 4. Growth recipes for simulation and experimentation: (a) top temperature, (b) bottom temperature.

3. Results and Discussion

Figure 5 shows the PL and IR results of bricks at positions No. 25–32 in the two experimental silicon ingots grown with different bottom temperatures. Figure 5(a.1,a.2) show that ingot 1 had interwoven inclusions at a height of about 150 mm in the middle and late stages of the crystallization process. The appearance of these interwoven inclusions is the same as that reported by Tang [4]. It is believed that the main components of the inclusions are silicon carbide and silicon nitride.

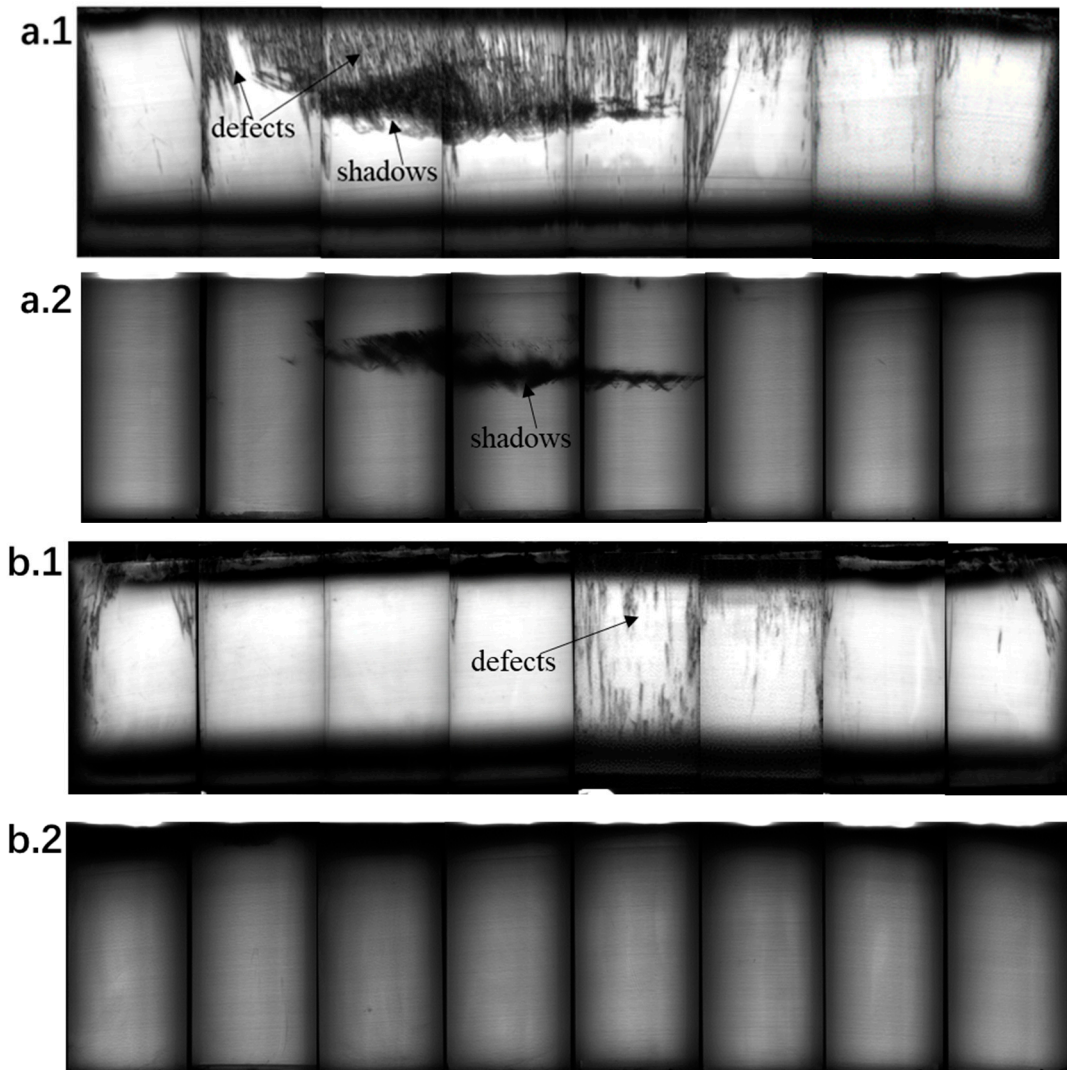


Figure 5. Side-view PL and IR images of bricks No. 25–32 of ingots (a.1,b.2) showing interwoven inclusions: PL results are shown in (a.1,b.1), while IR results are shown in (a.2,b.2).

Figure 5(b.1,b.2) show that no inclusions were found in ingot 2, and the black area at the top of ingot 2 was thicker than that of the other ingots. Analysis confirms the absence of visible inclusions in ingot 2, thereby confirming its purity. However, it is noteworthy that the dark area at the top of ingot 2 appears more pronounced than similar regions in the other ingots, suggesting potential variances in material properties or the presence of impurities in that particular area.

The utilization of PL imaging facilitates a thorough examination of the luminescent characteristics of the sample, enabling the detection of defects and inclusions. Conversely, IR imaging is tailored to pinpoint inclusions and evaluate the sample's transparency to infrared light. Integrating these two methodologies offers a multifaceted approach to characterizing silicon bricks, enhancing the precision and accuracy of identifying different

imperfections and contaminants. Defects and inclusions can be displayed in the PL results, while only inclusions can be seen in the IR results [18,19].

The simulation results of the silicon melt flow during the growth process of the two experimental ingots cast with different bottom temperatures are shown in Figure 6. Figure 6 gives the simulation results of the temperature distribution and silicon melt flow near the solid–liquid heights of 150 mm and 200 mm, where inclusions usually appear, for the two experimental silicon ingot growth processes. The flow of the silicon melt is indicated by arrows. The direction of the arrow represents the direction of the melted silicon’s flow. The longer the arrow, the greater the flow velocity of the melt flow. As shown in the red dashed box in Figure 6, the flow direction of the silicon melt near the solid–liquid interface in the growth process of silicon ingot 2 is mainly upward and horizontal, while the flow direction of the silicon melt in silicon ingot 1 is mainly downward and horizontal. In addition, the flow velocity of the melt at the solid–liquid interface in silicon ingot 2 is greater than that in silicon ingot 1. In the right part of Figure 6, it is clear that the temperature of the melted silicon near the solid–liquid interface of silicon ingot 2 is higher than that of silicon ingot 1. The diffusion coefficient of impurities such as nitrogen and carbon, which form inclusions, increases with temperature in the silicon melt [19,20]. Therefore, the impurities are more likely to flow with the flow of the melt in higher–melt–temperature environments. It can be seen that the melted silicon near the solid–liquid interface in silicon ingots grown at high bottom temperatures has a stronger upward melt flow, which can carry impurities and transport them upwards to the zone with higher temperature, away from the zone with lower temperature near the solid–liquid interface, thereby reducing the risk of inclusion formation near the low–temperature zone near the solid–liquid interface.

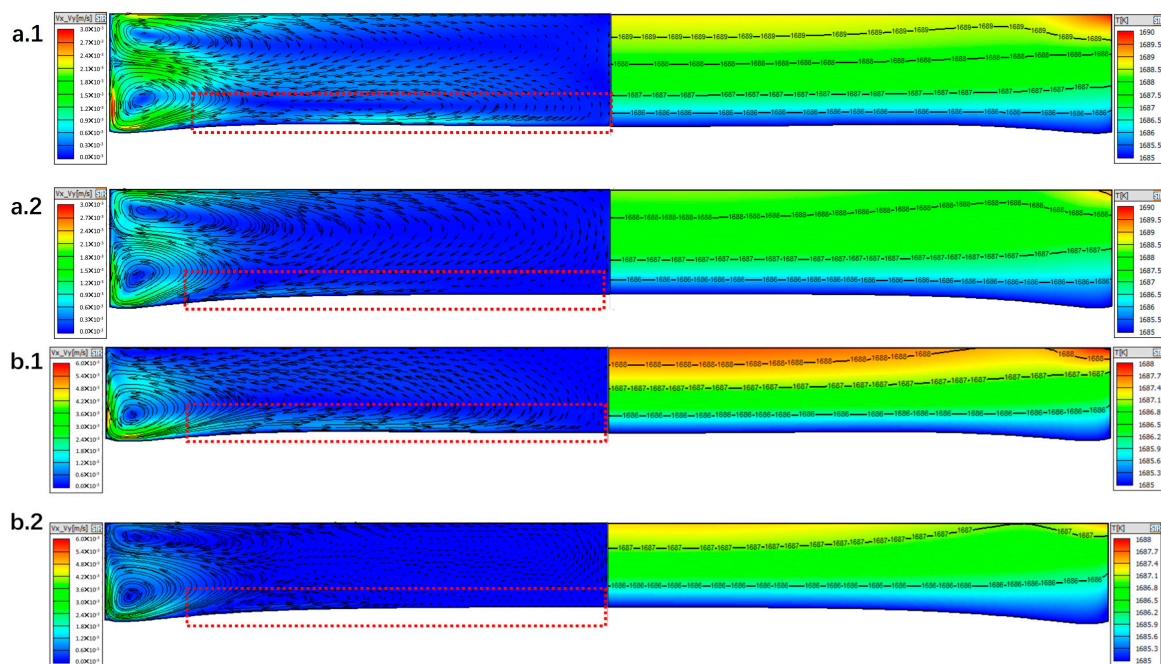


Figure 6. Simulation results of melt flow (left) and temperature distribution (right) of 150 mm growth height (a1,a2) and 200 mm growth height (b1,b2), (a1,b1) lower longitudinal temperature gradients, (a2,b2) conventional longitudinal temperature gradients.

4. Conclusions

In this paper, we investigated the disappearance of interwoven inclusions in two silicon ingots cast using different growth processes. We meticulously compared the longitudinal temperature gradients sustained within these ingots during their growth stages to unveil the factors causing the dissolution of inclusions. Our results indicate a connection between the removal of these inclusions and a heightened temperature at the base of the ingots.

The reduced temperature difference along the length, along with a steady top temperature and increased bottom temperature, is believed to promote a stronger upward movement of the molten silicon during ingot growth. This adjusted thermal pattern probably aids in moving impurities towards the upper sections of the ingot, rather than allowing them to accumulate and form inclusion bodies near the solid–liquid boundary. The improved temperature conditions within the molten silicon are thought to boost impurity transport efficiency, hence lowering the chances of inclusion formation and leading to a purer crystalline silicon structure.

These findings underscore the significance of meticulous regulation of temperature gradients throughout the crystal growth process, given its impact on the fluid dynamics of the melt and, consequently, the dispersion and separation of impurities within silicon ingots. The practical applications of this study can offer valuable insights for refining casting protocols to improve material quality in semiconductor production.

Author Contributions: Conceptualization, L.L. and C.F.; methodology, L.L.; software, L.L.; validation, L.L.; formal analysis, L.L.; investigation, L.L.; resources, L.L.; data curation, L.L.; writing—original draft preparation, L.L.; writing—review and editing, L.L. and C.F.; visualization, L.L. and C.F.; supervision, L.L. and C.F.; project administration, L.L.; funding acquisition, C.F. All authors have read and agreed to the published version of the manuscript.

Funding: This work is supported by the National Nature Science Foundation of China (Grant No. 12235003) and also by the National Key R&D Program of China (Grant No. 2023YFA1606900).

Data Availability Statement: The original contributions presented in the study are included in the article; further inquiries can be directed to the corresponding authors.

Conflicts of Interest: The authors declare no conflicts of interest. The funders had no role in the design of the study; in the collection, analyses, or interpretation of data; in the writing of the manuscript; or in the decision to publish the results.

References

1. Li, W.-C.; Tsai, D.-M. Automatic saw–mark detection in multicrystalline solar wafer images. *Sol. Energy Mater. Sol. Cells* **2011**, *95*, 2206–2220. [[CrossRef](#)]
2. Qiu, J.; Li, X.; Zhang, S. Research on an improved bath cooling and lubrication method for diamond wire sawing. *Int. J. Adv. Manuf. Technol.* **2021**, *112*, 2123–2132. [[CrossRef](#)]
3. Zhou, N.; Liu, S.; Zhou, P.; Lei, Q.; Zhou, L. A Study on Characterization and Prevention of Shadows in Cast Mono-Crystalline Silicon Ingots. *Cryst. Res. Technol.* **2022**, *57*, 2100205. [[CrossRef](#)]
4. Tang, S.; Qi, X.; Chang, C.; Wang, Q.; Liu, L. Analysis of the formation of interweaved strips in cast quasi–single crystal silicon ingots. *J. Cryst. Growth* **2023**, *622*, 127401. [[CrossRef](#)]
5. Tsoutsouva, M.; Oliveira, V.A.; Camel, D.; Thi, T.N.T.; Baruchel, J.; Marie, B.; Lafford, T.A. Segregation, precipitation and dislocation generation between seeds in directionally solidified mono–like silicon for photovoltaic applications. *J. Cryst. Growth* **2014**, *401*, 397–403. [[CrossRef](#)]
6. Liu, S.; Xia, M.; Chen, F.; Lei, Q. Analysis of the Characterization of Impurities and Defects in Cast Monocrystalline Silicon with Shadows. *Silicon* **2023**, *15*, 1393–1400. [[CrossRef](#)]
7. Davis, J.R.; Rohatgi, A.; Hopkins, R.H.; Blais, P.D.; Rai–Choudhury, P.; McCormick, J.R.; Mollenkopf, H.C. Impurities in silicon solar cells. *IEEE Trans. Electron Devices* **1980**, *27*, 677–687. [[CrossRef](#)]
8. Zhang, Z.; Huang, Q.; Huang, Z.; Li, B.; Chen, X. Analysis of microcrystal formation in DS–silicon ingot. *Sci. China Technol. Sci.* **2011**, *54*, 1475–1480. [[CrossRef](#)]
9. Matsuo, H.; Ganesh, R.B.; Nakano, S.; Liu, L.; Arafune, K.; Ohshita, Y.; Yamaguchi, M.; Kakimoto, K. Analysis of oxygen incorporation in unidirectionally solidified multicrystalline silicon for solar cells. *J. Cryst. Growth* **2007**, *310*, 2204–2208. [[CrossRef](#)]
10. Liu, L.J.; Nakano, S.; Kakimoto, K. Carbon concentration and particle precipitation during directional solidification of multi–crystalline silicon for solar cells. *J. Cryst. Growth* **2008**, *310*, 2192–2197. [[CrossRef](#)]
11. Li, Z.Y.; Liu, L.J.; Ma, W.C.; Kakimoto, K. Effects of Argon Flow on Heat Transfer in a Directional Solidification Process for Silicon Solar Cells. *J. Cryst. Growth* **2011**, *318*, 298–303. [[CrossRef](#)]
12. Li, Z.Y.; Liu, L.J.; Ma, W.C.; Kakimoto, K. Effects of Argon Flow on Impurities Transport in a Directional Solidification Furnace for Silicon Solar Cells. *J. Cryst. Growth* **2011**, *318*, 304–312. [[CrossRef](#)]
13. Li, Z.Y.; Liu, L.J.; Liu, X.; Zhang, Y.F.; Xiong, J.F. Effects of argon flow on melt convection and interface shape in a directional solidification process for an industrial–size solar silicon ingot. *J. Cryst. Growth* **2012**, *360*, 87–91. [[CrossRef](#)]

14. Teng, Y.-Y.; Chen, J.-C.; Huang, B.-S.; Chang, C.-H. Numerical simulation of impurity transport under the effect of a gas flow guidance device during the growth of multicrystalline silicon ingots by the directional solidification process. *J. Cryst. Growth* **2014**, *385*, 1–8. [[CrossRef](#)]
15. Tang, S.; Luo, J.; Chang, C.; Wang, Q.; Liu, L. A new form of impurity cluster in casting quasi-single crystalline silicon. *J. Cryst. Growth* **2022**, *590*, 126704. [[CrossRef](#)]
16. Tang, S.; Qi, X.; Chang, C.; Wang, Q.; Liu, L. Application of a new grain boundary technology for quasi-single crystalline silicon ingots. *J. Cryst. Growth* **2023**, *607*, 127109. [[CrossRef](#)]
17. *GB/T 13584–2011; Measuring Methods for Parameters of Infrared Detectors*. Ministry of Industry and Information Technology (Electronics) Publishing House: Beijing, China, 2011.
18. Binetti, S.O. Photoluminescence and Infrared Spectroscopy for Impurities Identification in Silicon for Photovoltaic Applications. Intervento Presentato a: School of Photovoltaic and Renewable Energy Engineering: Public Research Seminars, Sydney, Australia. 2019. Available online: <https://www.engineering.unsw.edu.au/energy-engineering/research/public-research-seminars> (accessed on 10 December 2023).
19. Luo, J.; Zhou, C.; Li, Q.; Lin, Y.; Liu, L. Atomic transport properties of silicon melt at high temperature. *J. Cryst. Growth* **2022**, *590*, 126701. [[CrossRef](#)]
20. Mostafa, A.; Medraj, M. Binary Phase Diagrams and Thermodynamic Properties of Silicon and Essential Doping Elements (Al, As, B, Bi, Ga, In, N, P, Sb and Tl). *Materials* **2017**, *10*, 676. [[CrossRef](#)] [[PubMed](#)]

Disclaimer/Publisher’s Note: The statements, opinions and data contained in all publications are solely those of the individual author(s) and contributor(s) and not of MDPI and/or the editor(s). MDPI and/or the editor(s) disclaim responsibility for any injury to people or property resulting from any ideas, methods, instructions or products referred to in the content.